Article

Not peer-reviewed version

Atmospheric Carbon Dioxide: A Fresh Look at Exchange Flux, Isotopic Carbon, Fossil Fuel Emissions and Residence Time

Stephen Taylor *

Posted Date: 19 March 2024

doi: 10.20944/preprints202205.0172.v2

Keywords: CO2 residence-time; CO2 lifetime; Anthropogenic Emissions; Revelle Factor; Exchange Flux; Bomb Pulse; Carbon Cycle; Airborne Fraction

 doi:10.20944/preprints202205.0172.v2

Article

Atmospheric Carbon Dioxide: A Fresh Look at Exchange Flux, Isotopic Carbon, Fossil Fuel Emissions and Residence Time

Stephen E. Taylor

Geomatix Ltd, UK; set@geomatix.net

Abstract: This paper presents a new implementation of a 2-box absolute flow model, enabling the calculation of CO_2 transfer between the atmosphere and a mixing reservoir representing the combined effect of the terrestrial and ocean regions. The model uses published values of anthropogenic CO_2 fossil fuel emissions (CO2ff), atmospheric CO_2 mixing ratio and nuclear weapons bomb yields, to compute atmospheric $\delta^{13}C$ and $\Delta^{14}C$ time-series. The level of agreement between the calculated values and the accepted values for $\delta^{13}C$ is within ± 0.05 ‰, and for $\Delta^{14}C$ is within ± 3‰, spanning 200 years. The model contains only seven internal parameters; these are varied to optimize the fit, leading to reasonable parameter values, indicating the validity of the method. In addition the model shows how a rising CO_2 exchange influx fluctuating with surface temperature is compatible with a nett atmospheric CO_2 sink. The study demonstrates that a single CO_2 residence time applies to both the ^{14}C bomb pulse and the anthropogenic flux, contrary to the conventional view that "bomb radiocarbon and anthropogenic CO_2 do not behave identically." [Joos 1994 Nature 370, 181–182]. It is shown that the difference in behaviour, claimed to be due to seawater chemistry, is not significant in practice since fluctuating bulk carbon dominates fluctuating isotopic ratio. A new analysis of the airborne fraction indicates that the assumption of a time-dependent exchange influx results in a similar residence time for bulk CO_2 as for ^{14}C in the nuclear bomb pulse, reinforcing the view that the ^{12}C, ^{13}C and ^{14}C carbon isotopic forms of CO_2 behave similarly in the carbon cycle.

Keywords: anthropogenic emissions; Revelle factor; exchange flux; bomb pulse; carbon cycle; airborne fraction

---

1. Introduction

The absolute (gross) size of the atmospheric CO_2 exchange flux between the atmosphere and the land/ocean are crucial in understanding the carbon cycle and estimating the effects of anthropogenic CO_2 fossil fuel emissions (CO2ff). As the Earth rotates daily and orbits the sun annually, the land and oceanic reservoirs cyclically "inhale" and "exhale" CO_2. These are the exchange fluxes, caused by corresponding changes in temperature, seawater solubility, photosynthesis, plant decay and respiration, resulting in a continuous cycle of absorption and emission. Within this complicated pattern of two-way fluxes, absorption occurs at one geographical location while simultaneously emitting at another. (IPCC Ed., 2001) This paper presents a means of determining the gross exchange flux. Measuring the gross exchange flux is more difficult than the task of finding its nett value, since the gross value does not contribute to the global carbon budget. Current estimates by the Global Carbon Budget (GCB) are for the land exchange flux 130 GtC yr^{-1}, and for the ocean flux 80 GtC yr^{-1} (Friedlingstein et. al., 2022). GCB refers its data source as being IPCC Canadell 2021 (IPCC Ed., 2021) who indicate that for the ocean, the gross figures originate from Figure 1 of Sarmiento & Gruber 2002 with applied corrections. Earlier GCB reports refer to IPCC (Ed) 2013 which states "Individual gross fluxes and their changes since the beginning of the Industrial Era have typical uncertainties of **more than 20%**" (author's highlight).

 doi:10.20944/preprints202205.0172.v2

In the 1970s attempts were made to model the carbon cycle and exchange flux using box models (e.g. Oeschger et al., 1975). Subsequently, General Circulation Models (GCMs) became common, since they could create global geographical distribution maps of the carbon-related processes despite requiring more computer resources. Although GCMs have been helpful in understanding the complexity of the global carbon cycle, box models, with their top-down simplification, offer specific advantages over the open-ended micro-accounting of GCMs. Such simpler models are "better testable" (Popper, 1934) and can help identify errors in formulation by focusing on the most significant factors. This paper presents a 2-box model that computes ^{14}C and ^{13}C isotopic ratios and differs from other box models in several ways. Firstly, its uses atmospheric CO_2 levels as input rather than output. Secondly, it employs absolute flow instead of net flow. Lastly, it incorporates a factor describing the proportion of fossil fuel emissions that are directly absorbed by sinks before dilution in the atmosphere takes place. The model accurately calculates $^{14}CO_2$ and $^{13}CO_2$ isotopic ratios spanning over 200 years, including the bomb pulse. Yet, notably, it uses the same residence time and reservoir mixing properties for ^{14}C, ^{13}C and ^{12}C.

In addition to uniquely providing estimates of the magnitude of the exchange flux, the method also challenges the widely held view that "*the atmospheric impulse response function of an isotopic perturbation decays much more rapidly than the impulse response function for bulk carbon"* (Heimann 1993). See Discussion Section 5.

1.1. Radiocarbon

The isotopic abundance of ^{13}C and ^{14}C present within atmospheric CO_2 is accurately known globally, with records going back hundreds of years. These isotopes have been measured in samples from tree rings (Stuiver & Quay 1981), ice cores (Rubino et al., 2013), and the atmosphere (Stuiver et al., 1998; D6). While ^{13}C is radioactively stable and forms around one percent of atmospheric carbon, ^{14}C undergoes radioactive decay with a half-life of 5700 ± 30 years (Kutschera 2013), and comprises about 1 part in 10^{12}. There is virtually no presence of ^{14}C in fossil fuel since it has all radioactively decayed. The $^{14}C/^{12}C$ ratio decreased between 1800 and 1960 because of dilution from rising fossil fuel emissions which are ^{14}C depleted, a process known as "Suess dilution" (Suess 1955). In 1960, atmospheric nuclear weapons testing began, causing a doubling of the absolute ^{14}C level within ten years. Since 1975 the level of ^{14}C has decreased (D6), partially due to washout from the exchange flow which contains a somewhat lower level of ^{14}C, but also because of "Suess dilution". Turning now to ^{13}C, its presence in fossil fuels is reduced when compared with the atmosphere, but only by around 2% (Stuiver and Polach, 1977). This small reduction arises from fractionation, which means the larger less mobile isotopic CO_2 molecules are less likely to become embedded in leaves and fossil carbon. Measurements show that the atmospheric $^{13}C/^{12}C$ ratio has decreased during the past 200-year period (D4), again partially due to dilution by fossil fuel carbon which contains the lower level of ^{13}C, and partially because of washout from the exchange flow. See Section 4.2.

2. CO_2 Absolute Flow Finite Reservoir Model

The model calculates the movement of CO_2 and its carbon isotopes between the atmosphere and a mixing reservoir, by calibration against isotopic measurements. The size of this mixing reservoir, and the exchange flux are "effective" values, combining the effect of the ocean and terrestrial origins. The concept of effective values is commonplace in the fields of engineering, applied science and economics. For example, economic inflation represents, in a single figure, the average of many different price increases on many items. Productivity measures the effective value created by each hour of work. Effective resistance in electronic engineering or hydraulics gives the overall resistance of a complex system to current or fluid flow. In each of these examples a single value is used to account for a property which is distributed throughout a complex system. The model presented is able to determine the effective values without requiring a detailed audit of the underlying constituent components, unlike other methods. The model consists of two boxes which are considered well-mixed, Figure 1. At each annual iteration, the isotopic mixing ratio within the reservoir and

 doi:10.20944/preprints202205.0172.v2

atmosphere changes because of incoming ^{13}C and ^{14}C. This change is calculated by the dilution formulae in Section 2.1. Using a similar notation as Tans et al.(1993) and Cawley (2011) we have

$$dC/dT = F_a + F_i - F_e \quad (1)$$

where C is the atmospheric carbon mass, F_a is the anthropogenic input flux from fossil fuel emissions, F_i, is the environmental flux flowing into the atmosphere and F_e is the environmental flux exiting the atmosphere. It is essential that F_i and F_e are kept separate because inflow and outflow are occurring in different places and they are needed to calculate the isotopic flows. Summing these components to form a nett flow would lose track of the separate isotopic mixing occurring across the globe.

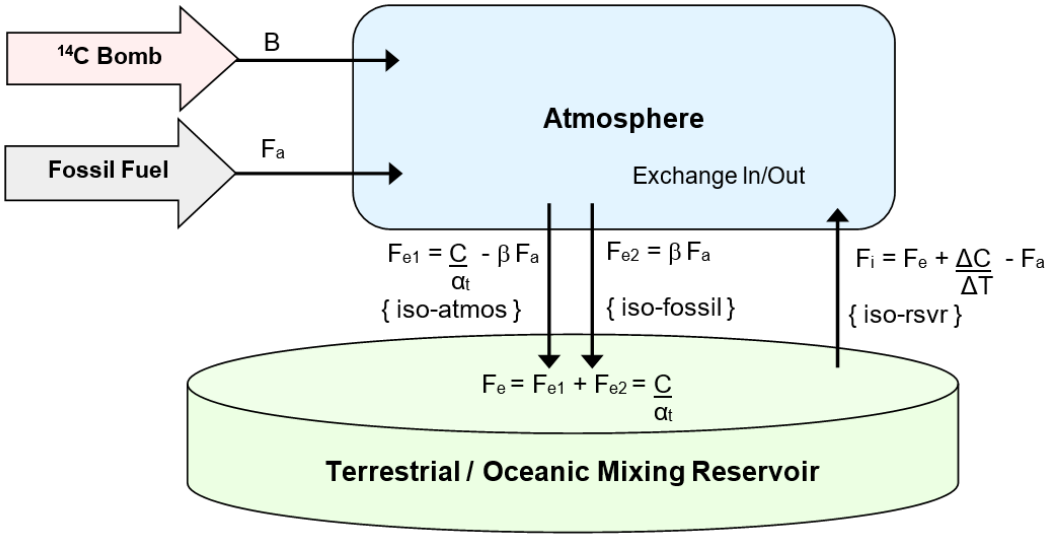

Figure 1. CO_2 Finite Reservoir Two-Box Model. The model describes the CO_2 flux between the reservoir and atmosphere, including its isotopic carbon contents. Anthropogenic fossil fuel CO2ff F_a, enters the atmosphere and a portion β exits without mixing. The remaining portion, (1-β) mixes into the atmosphere. Otherwise, full isotopic mixing is assumed to occur within each of the two storage regions, atmosphere and reservoir. At each iteration, the CO_2 flux outflow, F_e is proportional to atmospheric CO_2, C(t); its isotopic level corresponds to a mixture of atmospheric and fossil content. The CO_2 influx, F_i is determined by using equation (1) below. Atomic weapons ^{14}C B(t) directly enters the atmosphere with the timing and amounts determined by historical records of individual atmospheric atomic weapons testing, and bomb yield.

We first need an expression which connects the atmospheric CO_2 mass C, to the outflow; F_e is an obvious choice, being

$$F_e = a\,C \quad (2)$$

Equation(2) meets the common sense requirements that the absolute exchange exit flux varies in proportion to C, and if C were to be zero, the exit flux, F_e would also be zero. Substituting (2) into (1), we obtain an ordinary differential equation (ODE) for absolute inflow as

$$F_i = a\,C + dC/dT - F_a \quad (3)$$

The formula also describes the analogous situation of the flow of water from a bucket with a hole of size related to a, and two input taps (faucets) one of which represents the environmental exchange inflow, F_i and the other represents fossil fuel inflow, F_a. In practice, for use with data series, we replace dC/dt with $\Delta C/\Delta T$ where ΔC is the difference of successive carbon atmospheric mass and ΔT is the time difference, leading directly to the implementation equations shown in Section 2.4. The formulation differs from those used by other authors in two important respects. First, the incoming flux, F_i is not assumed constant and is calculated at each iteration by "balancing the books". Second, F_e is calculated by direct proportionality to the atmospheric CO_2 mass. As a consequence the model is not a predictive model of CO_2 atmospheric level. However, a great advantage of this formulation is that it enables the inflow to be calculated from measured data, eliminating the need to provide a

 doi:10.20944/preprints202205.0172.v2

bottom-up audit of individual CO_2 sources. Furthermore it provides estimates of CO_2 inflow and CO_2 isotopic ratios, and it computes a value for the CO_2 residence time constant. This constant applies equally to all three carbon species $^{14}CO_2$, $^{13}CO_2$ and $^{12}CO_2$. See Section 5.0 for further discussion.

The model uses a bomb yield multiplication factor, Y_b, as one of its seven optimisation parameters, to calculate the nuclear bomb yield of ^{14}C each year, $B_{14}[i]$. The bomb yield in megatons is obtained from records of atomic weapons atmospheric test detonations [D5]. A simple time delay of one year was used to allow for atmospheric mixing. The initial values i.e. $\delta^{13}C_{init}$, $\Delta^{14}C_{init}$, are also optimisation parameters within the model and determine the initial level of the curves in Figures 3 & 4, while the parameter $\delta^{13}C_{FF}$ determines the curve slopes in Figure 5.

2.1. Mass-Balance and Isotopic Dilution

If a number of gases are mixed but do not react, and each component gas, i, has a mass M_i, then from the law of conservation of mass (also known as Mass Balance)

$$M_T = \Sigma\, M_i$$

If within each component gas there is a specific molecule present in a ratio to its mass, R_i, then, since that specific molecule is conserved, the resulting mixture (e.g. paint mixing) having mass M_T has a ratio R_T given by

$$R_T = \Sigma\, R_i\, M_i / M_T \qquad (4)$$

Equation(4) also applies to the situation of mixing of isotopic gases. For practical reasons associated with historical measurements of radioactivity, studies of isotopic mixtures normally utilize the ratio of the sample activity, A_S to a standard sample activity A_{abs}, this ratio being known as the relative specific activity, A. Its value is then offset by one to provide the radioactivity scale, δ written (see Strenstrom 2011) in the form

$$\delta = (A_s/A_{abs}) - 1 = A - 1 \qquad (5)$$

In this scale, although δ increases linearly with As, its value is offset to be zero at the value of the absolute standard (often chosen to approximate background level), as for example in the cases of δ13C and δ14C. Applying (5) and substituting ASi for each component Ri of the mixture, leads after some algebraic manipulation, to

$$\delta_T = \Sigma\, (\delta_i\, M_i\,) / M_T \qquad (6)$$

The similarity with equation(4) shows that although δ is defined by an offset ratio scale we can still directly apply equation(6) to calculate the resulting value of δ_T for the mixture. The above scheme forms the basis for the system of equations $A_{14}[]$, $R_{14}[]$, $A_{FF}[]$ and $R_{FF}[]$ shown in the implementation Section 2.4 below.

2.2. Fractionation

The model generates values of $\delta^{14}C$, but we require $\Delta^{14}C$ for comparison with observed $\Delta^{14}C$ values. $\Delta^{14}C$ incorporates a fractionation correction to "translate the measured activity to the activity the sample would have had if it had been wood" (Strenstrom 2011). The correction formulae, which are themselves a function of $\delta^{13}C$, may be derived from equations by Strenstrom 2011 using equations 25, 28, 38, or Stuiver & Polach 1977 p356, 360, Table 1, where A_{SN} is the normalised specific sample activity, A_s is the specific activity of the atmosphere or reservoir, A_{abs} is the absolute specific standard, $\delta^{13}C_M$ is the ^{13}C sample measurement, and $\delta^{13}C_W$ is the ^{13}C standard for wood, giving

$$\delta^{14}C = A_S / A_{abs} - 1$$

$$\Delta^{14}C = A_{SN} / A_{abs} - 1$$

$$A_{SN} = A_S\, [\, (\, 1 + \delta^{13}C_W) / (\, 1 + \delta^{13}C_M)\,]^2$$

Eliminating A_S, A_{abs} and A_{SN} gives

 doi:10.20944/preprints202205.0172.v2

$$\Delta^{14}C = [1 + \delta^{14}C\ ]\ [\ (1 + \delta^{13}C_W) / (1 + \delta^{13}C_M)\ ]^2 - 1$$

The above formula was used to convert values of $\delta^{14}C$ computed by the model to $\Delta^{14}C$. The standard value of $\delta^{13}C$ for wood was taken as 25‰, while $\delta^{13}C_M$ was taken from the model. The correction was small, approximately 10‰ when the bomb pulse has a peak value of 800‰, decreasing to 0.03‰ when $\delta^{14}C$ approaches its background value of zero.

2.3. Age Correction

The radioactive decay of ^{14}C over the period from 1820 to 2020 is approximately 2%, since its half-life is 5700 ±30 years (Kutschera, W., 2013). However, this relatively small value is even less significant when one considers that the steady production of stratospheric ^{14}C approximately balances the amount of ^{14}C decay, since the two are in quasi-equilibrium. Therefore, neither ^{14}C decay nor natural stratospheric ^{14}C production were included in the model.

2.4. Implementation

Using equations 1-3 for the amount of CO_2 in the atmosphere C, its removal time α_t, the atmosphere outflow F_e, the inflow F_i, and the amount of CO_2 in the reservoir R, with the square brackets '[i]' referring to the value at each iteration i, we have

$$F_e[i] = C[i] / \alpha_t\ ,\ F_{e2}[i] = \beta\, F_a[i]\ ,F_{e1}[i] = F_e[i] - \beta\, F_a[i]$$

$$F_i[i] = F_e\ [i] + C\ [i] - C\ [i\text{-}1] - F_a\ [i\text{-}1]\ ,R[i] = R\ [i\text{-}1] + F_e[i] - F_i[i]$$

The ratio of ^{14}C to C in the atmosphere is denoted by A_{14} and in the reservoir by R_{14} and is calculated as follows. The new amount is given by the previous amount added to the input amounts with the output amount being subtracted, all divided by the total mass (see equation 4). If necessary we include the annual ^{14}C production due to atomic weapons bomb input, B_{14}. Hence we obtain

$$A_{14}[i] = (A_{14}[i\text{-}1]\ .\ C[i\text{-}1] + F_i[i\text{-}1].R_{14}[i\text{-}1] - F_e[i\text{-}1].A_{14}[i\text{-}1] + B_{14}[i\text{-}1]) / C\ [i]$$

$$R_{14}[i] = (R_{14}[i\text{-}1]\ .\ R[i\text{-}1] - F_i[i\text{-}1].R_{14}[i\text{-}1] + F_{e1}[i\text{-}1].A_{14}[i\text{-}1]\ ) / R\ [i]$$

Similarly, the relative atmospheric and reservoir fossil fuel content A_{FF} and R_{FF}, are calculated on a scale of 0 to 1 using the values at the previous iteration levels, where A refers to the atmosphere, and R the reservoir and subscripts FL means fossil fuel level, and NL means natural non-fossil level,

$$A_{FF}[i] = (A_{FF}\ [i\text{-}1].C[i\text{-}1] + F_i[i\text{-}1].R_{FF}\ [i\text{-}1] - F_{e1}[i\text{-}1].A_{FF}[i\text{-}1] - F_{e2}[i\text{-}1] + F_a\ [i\text{-}1])/C\ [i]$$

$$R_{FF}[i] = (R_{FF}\ [i\text{-}1].R\ [i\text{-}1] - F_i[i\text{-}1].R_{FF}\ [i\text{-}1] + F_{e1}[i\text{-}1].A_{FF}[i\text{-}1] + F_{e2}[i\text{-}1]) / R\ [i]$$

$$A_{FL}[i] = C[i]\ A_{FF}[i], \qquad A_{NL}[i] = C[i] - A_{FF}[i]$$

$$R_{FL}[i] = R[i]\ R_{FF}[i]\ ,\ R_{NL}[i] = R[i] - R_{FF}[i]$$

The offset isotopic ratiometric measure for ^{13}C is $\delta^{13}C$ and that for ^{14}C is $\Delta^{14}C$. These are calculated from the iterative series by:-

$$\delta^{13}C = \delta^{13}C_{FF}\ .\ A_{FF} + \delta^{13}C_N\ (1 - A_{FF}), \quad \Delta^{14}C = (A_{14} - 1)$$

Initial Conditions: $F_i[0] = F_e[0]\ ,\ A_{14}\ [0] = 1\ ,\ R_{14}\ [0] = 1,\ A_{FF}[0] = 0\ ,\ R_{FF}[0] = 0$

It is not necessary to embed a formula for attenuation factor, as discussed by Stuiver & Quay (1981), or for Suess dilution (Suess 1955) because they are implicitly represented.

3. Method

The input data between 1750 and 2020 was selected from the appropriate data source listing (D1-D6) and entered into a spreadsheet. The cell formulae were set to correspond to those equations in Section 2.4

 doi:10.20944/preprints202205.0172.v2

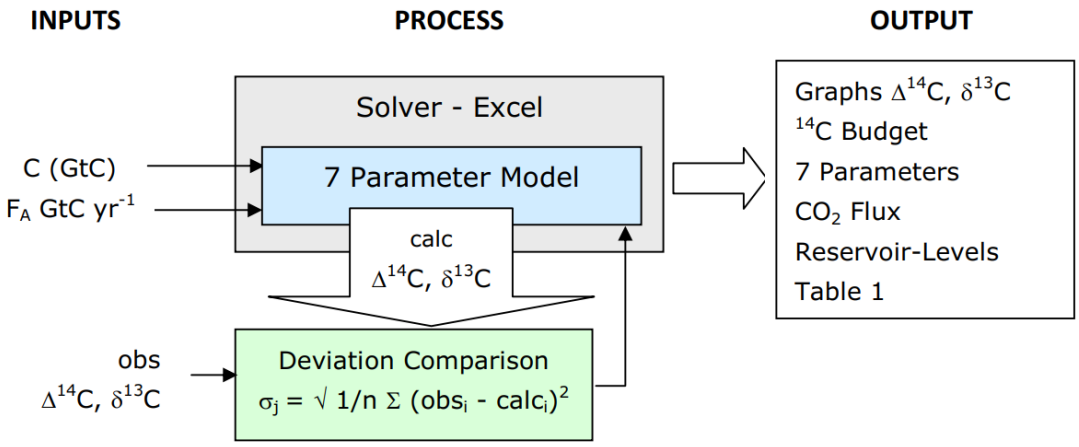

Figure 2. Solution Optimisation. The 7 parameter model and the deviation comparison formulae are implemented as cell formulae within Microsoft Excel. The deviation comparison formulae compares the measured time-series values of atmospheric Δ14C and δ13C with the calculated values. The Add-In Solver was used to numerically minimise the standard deviation by varying the values of the 7 parameters, providing the above outputs shown below in this study.

The optimisation-solution process is shown in Figure 2 above. The standard deviation between observed and predicted values, σ_1, σ_2 were determined for $\Delta^{14}C$ and $\delta^{13}C$ respectively. The values of $\Delta^{14}C$ between 1950 and 1968 were excluded from the summation because of the bomb pulse transient. The square root of the product of the standard deviations gives the overall geometric mean standard deviation, σ_T, hence

$$\sigma_j = \sqrt{1/n \, \Sigma \, (obs_i - calc_i)^2} \qquad (7)$$

$$\sigma_T = (\sigma_1 \times \sigma_2)^{1/2} \qquad (8)$$

The solver system was set to optimise the 7 parameters shown in Table 1 using the default solver options. The optimal solution was found by minimizing the discrepancy, σ_T using the standard "Solver" function of Microsoft Excel. The model has been tested using Microsoft Excel 2002 Version 10 and Microsoft Excel for Microsoft 365 MSO Version 2306 producing identical results.

4. Results

The results are in three main categories; the optimised seven parameters, the isotopic series, and the flux time series.

4.1. Parameter Values

Table 1 lists all seven parameter values along with their estimated errors. The error values were derived by varying each parameter up and down, while keeping the other parameter values constant, until the overall geometric mean standard deviation, σ_T approximately doubled. The error figure presented in the table is the mean of the two variations.

 doi:10.20944/preprints202205.0172.v2

Table 1. Solved 7 Parameter Values.

Parameter	**Sym.**	**Value**	**err.**
Residence time (years)	α_t	14.21	1.7
Reservoir Size rel. to Atmosphere 1750	RCO2	6.18	1.4
CO2ff Unmixed Uptake Factor	β	0.43	0.1
Atomic Bomb Yield: ^{14}C/MT ‰	Yb	1.61	0.1
Pre-industrial ^{14}C ‰	Δ^{14}Cinit	-3.2	10
Pre-industrial ^{13}C ‰	δ^{13}Cinit	-6.7	0.2
Fossil fuel ^{13}C ‰	δ^{13}Cff	-20.1	4

1) Residence Time

This compares favourably with Revelle & Suess (1957) of approximately 10 years, and Arnold (1957) of 10-20 years. It has subsequently been stated that "No single lifetime can be defined for CO_2.." (IPCC (Ed.): 2001, Table 1 p38). This study finds to the contrary.

2) Reservoir Size rel. to Atmosphere (1750)

The value for reservoir size are reported in IPCC Ed., (2013) in GtC as vegetation 450 to 650, soils 1500 to 2400, permafrost 1700, and surface ocean 900, corresponding to a range of 4550 to 5650. This study finds a reservoir size in GtC of 6.18 x 589 = 3640 GtC increasing to 3809 GtC in 2020 with errors of +/- 22%.

3) CO_2 Relative Unmixed Uptake

This study determines the quantity of CO2ff entering the sink without mixing in the atmosphere. Factor β accounts for the unmixed uptake, corresponding to that portion of the CO2ff emissions which directly enter the terrestrial/oceanic mixing reservoir. The effect of entry of pure undiluted CO2ff is a lowering of the ^{14}C and ^{13}C curves. The model finds that around 43% of CO2ff exits before mixing while 57% becomes fully mixed. A recent study has revealed that plants near nuclear power stations can uptake significant quantities of $^{14}CO_2$ (Naegler & Levin 2006). A study of urban grasses near a major highway revealed plants were composed of up to 13% of fossil-fuel carbon (Lichtfouse et al, 2005; Ota et al 2016). According to Kuderer et al (2018), "*The 14C signals from such point sources are well detectable in plant samples*". Since most fossil fuel emission sources are located near the land or ocean surface, it is reasonable to propose that a significant portion of CO_2 fossil fuel emissions are absorbed before fully mixing in the atmosphere.

4) Nuclear Bomb Yield

The model returned a value of 1.6 ± 0.1‰ of ^{14}C per MT for the nuclear bomb yield, with a total bomb yield of 440MT. For comparison, we convert the figures to ^{14}C atoms per MT bomb yield using formulae derived from Svetlik (2010) and Strensom (2011). The weight of carbon atoms, A_{CO2} in the atmosphere in 1950, when the CO_2 mixing-ratio was 312.8 ppm, was 664.43 GtC. The number of carbon atoms is given in terms of the molecular weight of naturally abundant carbon, MC = 12.01, and Avogadro's number $N_A = 6.022\times10^{23}$ by

$$NC = A_{CO2} \times N_A / MC.$$

The $^{14}C/C$ ratio $R^{14}C$ can be obtained from the specific activity, α = 0.226 Bq per gram, ^{14}C half life $T_{1/2}$ = 5730 years = 1.807 10^{11} s, molar weight of ^{14}C is M_{C14} = 14, and ln(2) = 0.6931, with

$$R^{14}C = a\ T_{1/2}\ M_{C14} / (N_A \times \ln(2)).$$

The number of ^{14}C atoms $N^{14}C$ created is given by the product of the two expressions giving

$$N^{14}C = NC \times R^{14}C = (A_{CO2} / MC) \times (a\ T_{1/2}\ MC_{14} / \ln(2)) = 4.6 \times 10^{28}.$$

Hence the number of 14C atoms per MT of bomb yield is 0.0016 x 4.6 x 10^{28} = 7.4 x 10^{25}, comparing favourably with reported values by Hesshaimer et al. (1994) of 1 to 2 x 10^{26} atoms per MT. The total bomb yield of 440MT gives a figure of 3.23 x 10^{28} atoms per MT, which compares with 6.1 x 10^{28} atoms per MT by Naegler & Levin (2006). The difference may be due to ^{14}C which is stored but does not mix in the biosphere or because of variation in bomb type and design.

 doi:10.20944/preprints202205.0172.v2

5) Isotopic Pre-Industrial Levels and Fossil Fuel Content

a) ^{14}C shows good agreement with Intcal20[D6] for 1820 of 0.7‰. For comparison the maximum level between 1820-2020 is 800‰.

b) ^{13}C initial value, shows excellent agreement with Rubino (2013) 1820 of $\delta^{13}C$ = 6.7‰.

c) $\delta^{13}C$ for CO2ff is slightly low as compared to figures reported by Stuiver & Polach (1977) for coal of $\delta^{13}C$ = -23 ‰.

4.2. Isotopic Time Series

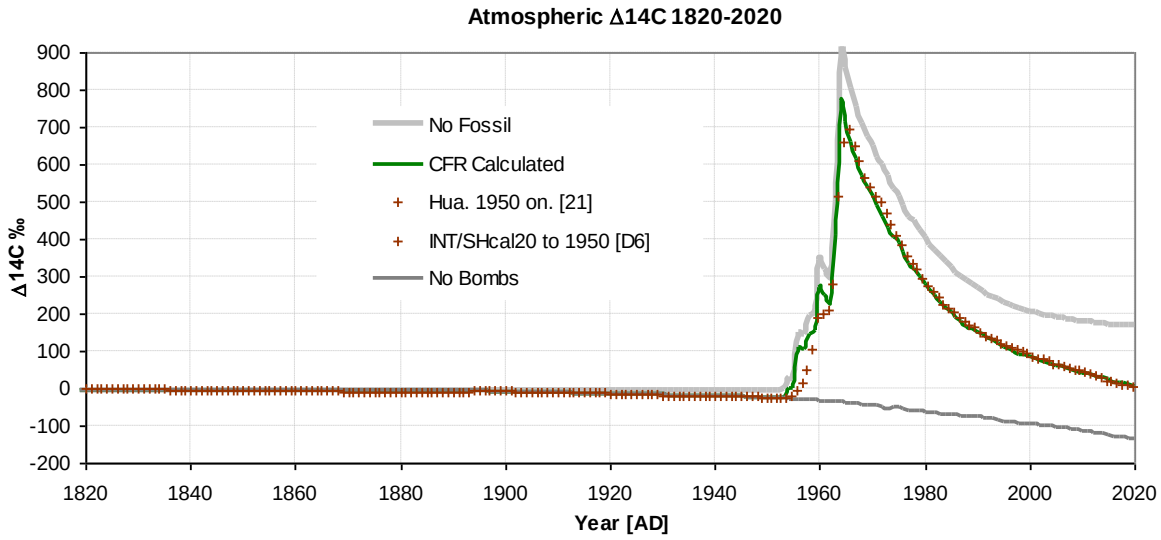

Figure 3. Atmospheric $\Delta^{14}C$ 1820-2020. showing 130 values before 1950 [D6] and 70 values from 1968 onwards (Hua et al.. 2022). Standard deviation between observed and predicted is σ = 3.01‰. For "no bombs" and "no fossil" see text.

Figures 3 & 4 display the actual and modelled $\Delta^{14}C$ values. The total number of observed data points used was 340, resulting in an overall standard deviation of 0.39‰. The quality of the fit is excellent, with a standard deviation of 3‰, corresponding to 0.4% of the range. In Figure 3, the slight decrease from 1820 to 1940 is due to Suess dilution, but the magnitude of the dilution is somewhat reduced by reservoir inflow, resulting in excellent agreement with the observations. Figure 4 shows the bomb pulse plotted as $\Delta^{14}C$. Initially, the pulse shape is a decaying exponential but, subsequently, due to Suess dilution and the re-emergence of ^{14}C from the mixing reservoir, the Δ14C decay shape becomes more linear. Despite these complicating factors, the predicted and observed values are in excellent agreement, indicating that the iteration formulae accurately handle the dilution and mixing processes. Figures 3 and 4 also show two hypothetical scenarios: "no bombs" and "no fossil". The "no bombs" scenario represents how the decrease would have continued without nuclear atmospheric weapons testing, while "no fossils" shows the situation without fossil fuel emissions. A recent work published by Graven et al. 2020 using a model originally produced by M. Heimann and R. Keeling and rewritten for Matlab, gave very similar results for "no bombs" and "no fossil" scenarios, further vindicating the model presented here and its approach.

Figure 5 shows the variation of $\delta^{13}C$ over 200 years, with predicted values showing a standard deviation of 0.05‰ from those observed, corresponding to 2.5% of the range. The steady reduction in $\delta^{13}C$ is caused by Suess dilution as fossil fuel emissions contain a lower level of ^{13}C, and by the re-emission of CO_2 from the reservoir. Again, this shape is accurately described by the iteration formulae.

 doi:10.20944/preprints202205.0172.v2

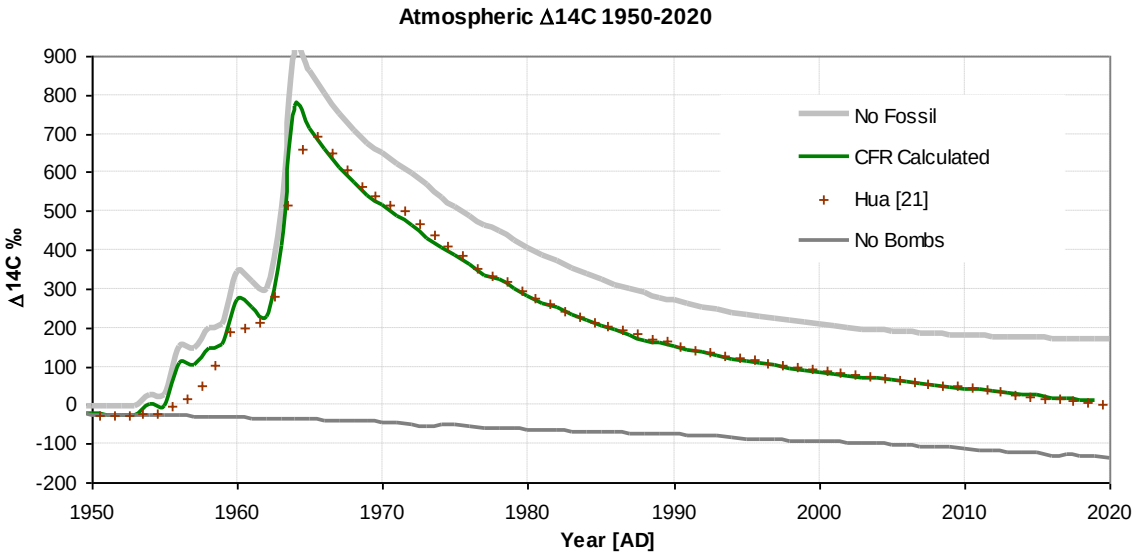

Figure 4. Atmospheric Δ14C between 1950 and 2020 showing the "bomb pulse" to 2020. For "no bombs" and "no fossil" see text.

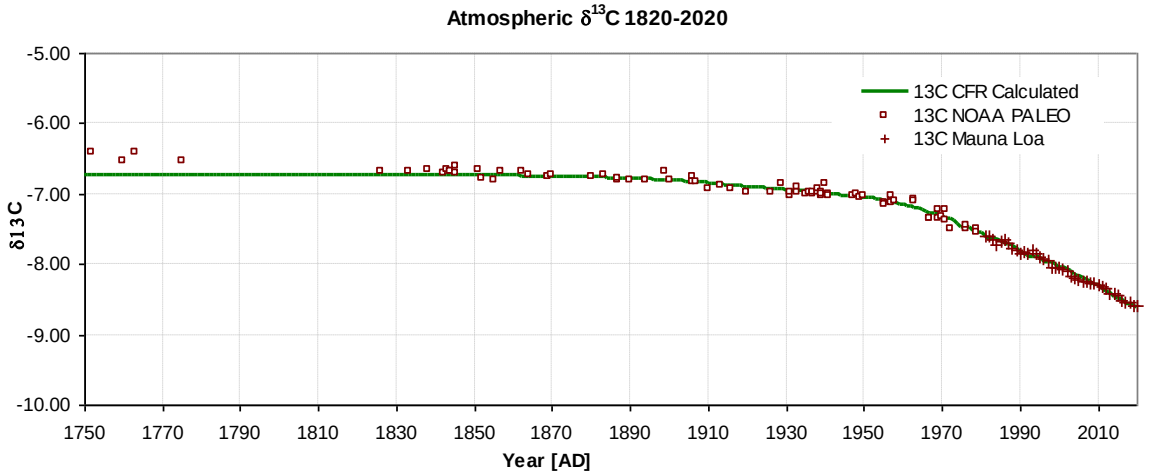

Figure 5. Atmospheric δ13C 1820-2020. Model calculated values: solid green, Observed NOAA Paleo [D4]: squares, Mauna Loa [D2]: crosses, $\sigma_{1820\text{-}2020}$= 0.05‰.

Inspection of the curve in Figure 4 reveals that atmospheric $\Delta^{14}C$ is decreasing to a value below its original background level. This decrease deviates from an exponential decay due to three main factors. a) Incoming fossil fuel emissions (free of ^{14}C) are diluting the atmosphere, this is commonly referred to as "Suess Dilution" (Suess 1955). b) Some of that fossil fuel emissions in the atmosphere is being washed out by the two way exchange flow. c) As time progresses, some of the incoming exchange flow has an increasing level of ^{14}C, because bomb ^{14}C has accumulated in the reservoir and is now being re-introduced to the atmosphere. If the effect (a) were the sole cause of the deviation of the bomb curve shape from a pure exponential decay, the curve would, by now, be well below the initial background. However, effect (b), the washout of fossil fuel emissions, raises the curve. This was noticed many years ago and termed by Stuiver and Quay (1981) the "attenuation factor". Effect (c) raises the tail slightly, further improving the fit in later years to the current level shown in Figure 4. Keeping track of all of these factors in a "back of the envelope" calculation is complex. The absolute flow model described in this study calculates at each iteration ^{13}C and ^{14}C in the reservoir and atmosphere (see Section 2.4). It does not need to explicitly consider Suess dilution, the Stuiver

 doi:10.20944/preprints202205.0172.v2

attenuation factor or flow-back since these emerge implicitly from the calculation embedded within the implementation equations (2.4)

4.3. Absolute 14CO2, Activity Concentration

The activity concentration of ^{14}C, which is its absolute amount rather than its ratio with C, is displayed in Figure 6. The graph shows how the activity concentration of ^{14}C in the atmosphere and the reservoir changes over time. The total amount of ^{14}C in the system is represented by the blue curve, while that in the atmosphere is shown in green. In 1960, atmospheric nuclear weapons testing caused a sudden step increase in the amount of ^{14}C. The atmospheric activity concentration shows the bomb pulse decaying to a minimum around 2000[AD] but then rising slightly again, this has been experimentally determined by Svetlik (2010). Some authors (e.g. Levin et al. 2010) have suggested ^{14}C industrial pollution may be a partial cause of the increase. However, this study accurately reproduces the ^{14}C curve without such a requirement. In this study, the increase in activity concentration can be attributed to $^{14}CO_2$ re-emerging from the mixing reservoir, while at the same time causing a slight drop in the reservoir level.

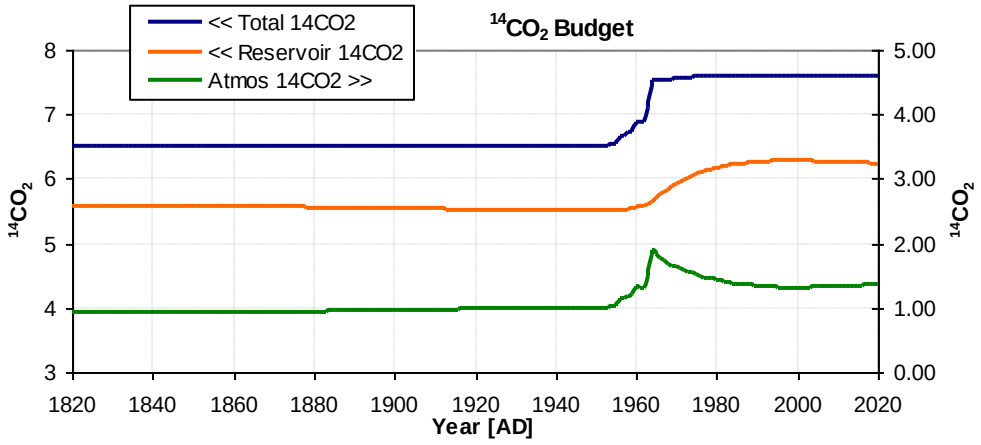

Figure 6. $^{14}CO2$ Budget. Model derived absolute $^{14}CO2$ (also known as activity concentration) for the reservoir (orange), the atmosphere (green), and their total (blue) in units relative to the $^{14}CO2$ content of the atmosphere in 1950. The total, being the sum of reservoir plus atmosphere, shows the near step function in $^{14}CO2$ created by nuclear atmospheric weapons testing. After the initial fall of atmospheric content, the small rise since 2000 is confirmed by the results of Svetlik (2010), see text.

4.4. Flux Time Series

The model calculates the mean gross exchange flux in 2019 as 60 GtC yr^{-1}, these are approximately 27% of the total IPCC figures (IPCC Ed., 2021 Fig 5.12) of 217 GtC yr^{-1}, and more closely resemble the ocean figures alone of 54 GtC yr-1. Why is there such a discrepancy? We propose here that it is related to the definition of exchange flux. In the real world, if the nett value of a significant two-way exchange flux is zero, it can only have an effect if it has mixed isotopically en route to and from the reservoir. If there is no isotopic mixing, the returned flux is identical to the original absorbed flux both in its bulk and isotopic content; its effect is therefore insignificant. Thus a portion of the exchange flux has no effect. To determine the "effective exchange flux", the model finds the size of the flux which when mixed in both the reservoir and atmosphere, minimises the discrepancy between its computed 13C and 14C curves and the experimentally determined values. This flux is different from the exchange flux of IPCC 2021, which includes cyclical flows of isotopically identical i.e. unmixed gas. This issue also influences the calculation of residence time, which is defined by "atmospheric mass/removal rate", and has been quoted by many in the field (Harvey 2000). The calculation provdes a figure of ~4 years, being obtained by dividing the atmospheric size of 871 GtC by the gross exchange flux of IPCC 2016 i.e. 217 GtC yr^{-1}. However, using the model-determined

 doi:10.20944/preprints202205.0172.v2

exchange flux of 60 GtC yr-1, we obtain 871/60 which yields a residence lifetime of ~14 years, similar to the observed decay of the bomb pulse. Because isotopic mixing occurs more readily within the ocean, it is therefore also unsurprising that the exchange figure from the model more closely resembles the ocean exchange figures rather than the terrestrial portion. See Discussion.

4.5. Influx and Temperature

The absolute inflow, computed by the model, is plotted from 1960 to 2020 in Figure 8. Essentially this is an expanded version of the green plot on Figure 7. The same graph also shows global temperature (D7) plotted on a suitable vertical scale, revealing that many of the temperature excursions match CO_2 inflow excursions. The correlation coefficient between the two plots is 0.94. Although correlation cannot be considered as causation, it is difficult to conceive of a mechanism whereby a global temperature change could be influenced by the rate of CO_2 inflow, rather than its absolute atmospheric mixing ratio. An obvious temperature-dependant mechanism for CO_2 gas release in the ocean is the decrease of solubility with temperature. On land the balance between productivity, respiration, decay and temerature has been discussed by Melillo et al. 2011. According to the model, from 1960, annual atmospheric inflow has increased by 12.7 GtC yr^{-1} while annual outflow has increased by 13.7 GtC yr^{-1}.

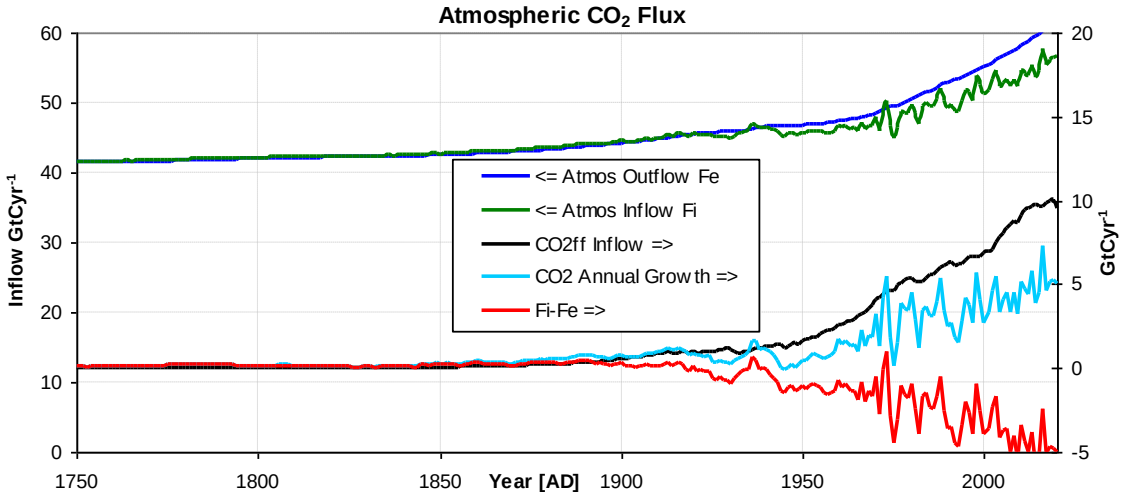

Figure 7. Output from the model showing:- Atmospheric Outflow (blue), Atmospheric Inflow(green), CO2ff Inflow (black) CO2 Atmospheric growth (light blue), and Fi-Fe, (red). The arrow on the legend indicates the relevant axis.

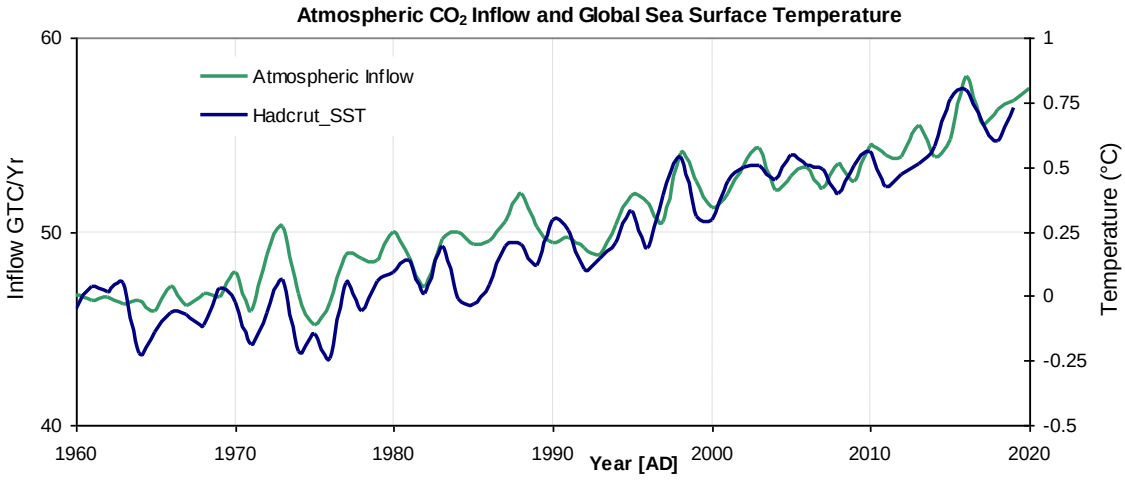

 doi:10.20944/preprints202205.0172.v2

Figure 8. CO_2 inflow (green) and observed global sea-surface temperature (blue) indicating a high degree of correlation of 0.94.

4.6. Cumulative Flux & Levels 1750-2020

Figure 9 shows the cumulative CO_2 flux and CO_2 levels over a period 270 years, during which, 453 GtC of CO2ff was supplied. Out of this, 282 GtC remains in the atmosphere, while 171 GtC is stored in the reservoir. However, the level of fossil sourced CO_2 increased by 120 GtC in the atmosphere and by 333 GtC in the reservoir, also totalling 453 GtC. Although these figures may seem inconsistent, there is no contradiction. The bulk figures indicate the amount of CO_2 without accounting for its isotopic composition. Fossil level is based upon isotopic content, which depends upon dilution caused by the size of the exchange flux in and out and its source and destination isotopic levels. The relative growth of the atmopsheric CO_2 level since 1750 is 48%. The relative level of fossil fuel emmissions within the atmosphere in 2020, isotpically tracked is 14% (See Rice 2022). In terms of bulk flow, there is a net outflux of 171 GtC from the atmosphere. Figure 7 shows that while both exchange outflow F_e (blue) and inflow F_i (green) are increasing, the outflow has increased more, confirming the nett uptake of CO_2 from the atmosphere by the terrestrial and ocean reservoirs.

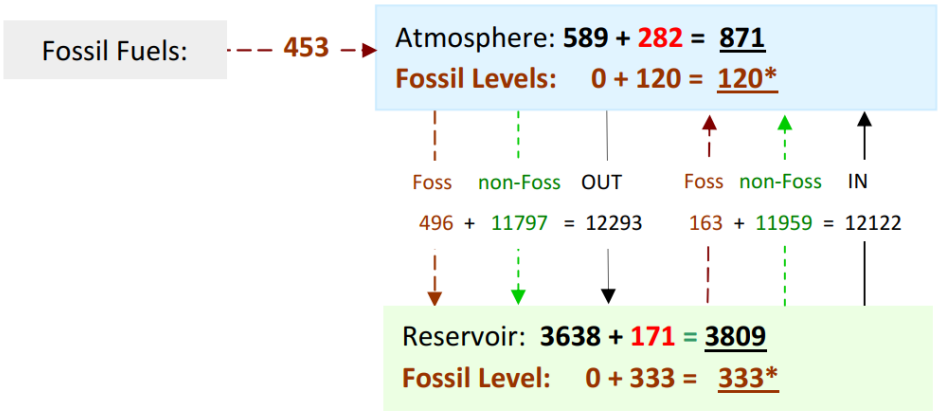

Figure 9. Cumulative CO_2 flux, between atmosphere and reservoirs levels over the period 1750-2020. Fossil fuel flux and fossil levels (identified by composition) are shown in brown, non-fossil flux are in green while total variation are shown in black with growth being shown in red. Final values (in 2020) are underlined. * As determined by isotopic tracking.

5. Discussion

This section provides further evidence challenging the current consensus view regarding CO_2 residence time summarised below. Comparing the oceanic uptake of isotopic CO_2 with the uptake of excess of CO_2 "Siegenthaler and Oeschger (1987) reported that, *"The isotopic perturbation vanishes faster than the CO_2 excess"*. The concept was discussed by Heimann in 1993 *"the atmospheric impulse response function of an isotopic perturbation decays much more rapidly than the impulse response function for bulk carbon."* Joos in 1994 reported *"bomb radiocarbon and anthropogenic CO2 do not behave identically."* Houghton 1996, IPCC explained *"an atmospheric perturbation in the isotopic ratio disappears much faster than the perturbation in the number of 14C atoms"*. Tans 2022 explains *"The Revelle factor does not apply to isotopic equilibration because a 12CO2 molecule is replaced by a 13CO2 or vice versa. As a result, an isotopic anomaly disappears from the atmosphere more quickly than a total CO2 anomaly."* We term here this concept as the "Revelle Bypass" for brevity. The following two sections provide further evidence that bomb radiocarbon and anthropogenic CO_2 ***do*** behave similarly within the atmosphere and carbon cycle, supporting the same clear implications derived from the model earlier in this paper, refuting the "Revelle Bypass". This position is not taken lightly, the author believes it is a necessary correction to climate science.

 doi:10.20944/preprints202205.0172.v2

5.1. Isotopic Behaviour

Following Tans' approach (Tans 1994, 2022) we see that a change in atmospheric ^{14}C concentration can arise in two ways; first from a change in concentration of atmospheric CO_2 even though the $^{14}C/C$ ratio remains constant (term A), and second, from a change in $^{14}C/C$ ratio while atmospheric CO_2 remains constant (term B). Hence, we have

$$\underset{A}{} \qquad \underset{B}{}$$

$$F14C = d(CR)/dt = R.dC/dt + C.dR/dt$$

The author believes Tans' application of this equation to the real world is flawed since Tans only derives the second term. However, the first term is highly significant. In the real world, there is no short-term daily equilibrium in CO_2, since it fluctuates diurnally as the Earth rotates, and the terrestrial /oceanic reservoirs cyclically and continuously exchange large quantities of CO_2. This CO_2 flux brings with it quantities of ^{14}C and ^{12}C, which constitute the first term A. The second term B, is driven by fluctuations in the $^{14}C/^{12}C$ ratio, such as from decaying vegetable matter which has previously preferential absorbed ^{12}C during photosynthesis. We can better estimate the magnitude of the contribution of variations of either term, by dividing both sides by CR giving

$$\underset{A}{} \quad \underset{B}{}$$

$$d(CR)/CR = dC/C + dR/R$$

where R is the isotopic ratio, and C is the amount of bulk carbon. The Revelle factor applies only to term A because it describes a change in bulk carbon; in doing so it applies to the various isotopes equally. A comparison of the local values of the relative sizes of dC/C and dR/R shows term A greatly dominates B. This can be determined by examination of a number of studies (e.g. Bishcof 1960, Dai et al. 2009, Faassen et al, 2022, Leinweber et al., 2009, Olsen et al. 2004, Palonen et al. 2018, Takahashi et al. 2002). The local variation dC/C was estimated from the above references as being of the order of ≈6 ppm/400ppm (≈0.015) per hour, while the variation dR/R for 14C estimated at most as around ≈8‰ (≈0.008) per hour and for 13C ≈ 0.2 ‰ (≈0.0002) per hour. Hence $|A|$ significantly dominates $|B|$. Therefore, it is irrelevant whether or not B has an ability to bypass carbonate chemistry (i.e. "Revelle Bypass") as claimed by many, since A is the dominant flux, and term A does not have the ability to preferentially bypass seawater chemistry for ^{14}C. Therefore in practice term A dominates B and both ^{12}C and ^{14}C are equally subject to the effects of seawater carbonate chemistry.

5.2. Airborne Fraction

The airborne fraction is defined as the ratio of atmospheric CO_2 growth to total CO_2 anthropgenic emissions (Friedlingstein 2022). Its relatively stable value of approximately one half was remarked upon by Broeker in 1975. It has been suggested that, since the rise in anthropogenic emissions is approximately exponential, this indicates that absorption of atmospheric CO_2 is governed by an ordinary differential equation (ODE) (Cawley 2011). We provide below the mathematical derivation of airborne fraction, AF from an ODE containing the bulk residence time, t_a and exponential rate-of-rise t_s of anthropogenic emissions, where $t_a = 1/a$ and $t_s = 1/s$. If fossil fuel emissions increase exponentially, F_a in equation (3) may be replaced with e^{st} as

$$dC/dt = -a\,C + F_i + e^{st} \qquad (13)$$

The particular solution for (13) is given by many authors, (Gilbert Strang MIT 2015), and shows the resulting response of CO_2 level (sometime called the "adjustment time") comprises the sum of two time exponentials as

$$C=(e^{st} - e^{-at})/(s+a) + C_0 \qquad (14)$$

The solution can be verified by substitution of (14) into (13), a step which shows that $aC_0 = F_i$ where C_0 represents the equilibrium value. The instantaneous airborne fraction, being defined as the ratio of the rate of rise of atmospheric CO_2 to the assumed exponentially increasing CO2ff input rate, can be found by dividing by e^{st}, which, after some manipulation, gives

$$AF = (dC/dt)/\,e^{st} \;=\; s/(s+a) \;+\; a\,e^{-(s+a)t}/(s+a) \;+ (F_i(t) - aC_0)\,e^{-st} \qquad (15)$$

 doi:10.20944/preprints202205.0172.v2

The first term represents the value to which the airborne fraction tends; the second represents a transient with negative exponent which rapidly diminishes, and the third represents the out of equilibrium contribution. If F_i is constant it balances the outgoing exchange flux, aC_0 setting the third term to zero and the first term of (15) is the value to which the AF settles. Putting $t_a = 1/a$ and $t_s = 1/s$ we can then write

$$AF \Rightarrow s/(s+a), \quad a \Rightarrow s(1/AF - 1), \quad t_a \Rightarrow t_s/(1/AF - 1) \qquad (16)$$

The formulae in (16) apply if F_i is constant and if the transient has settled; it also applies to cumulative values. Typical values are AF=0.45, t_s=53 years, (Cawley 2011) giving t_a a value 43 years. The difference in value between this and the bomb pulse decay time (by at least a factor of 3), has been quoted as supporting evidence that the "Revelle Bypass" applies (Harvey 2000). However if F_i is not constant, as is the case in practice, the calculation of AF must use equation (15) rather than the simplified form equation (16), returning a different value. IPCC 2021, in AR6 figure 5.12, shows values of F_i from 1750 rising for land by 25.6 GtC yr^{-1} and for ocean 23.0 GtC yr^{-1}. Similar rising values of F_i are also shown by the model presented in this study, which reports its rise from 41.5 GtC yr^{-1} to 56.7 GtC yr^{-1}, see Figure 8. Applying this rising sequence of F_i to equation (13) with a time constant of 14.2 years yields the resulting time-series shown graphically Figure 10 below. Thus the time constant differs significantly from the value of 43 years which was obtained when F_i was incorrectly assumed to be constant. The longer time constant therefore does not indicate that the "Revelle Bypass" applies, but rather indicates it is an incorrect result caused by ignoring the rising value of F_i. The equation was also solved using an exponential fit to the fossil fuel emissions rather than the emissions themselves giving the similar plot shown in green. The similarity of the plots shows there is no need to invoke the "Revelle Bypass" in order to account for differing time constants.

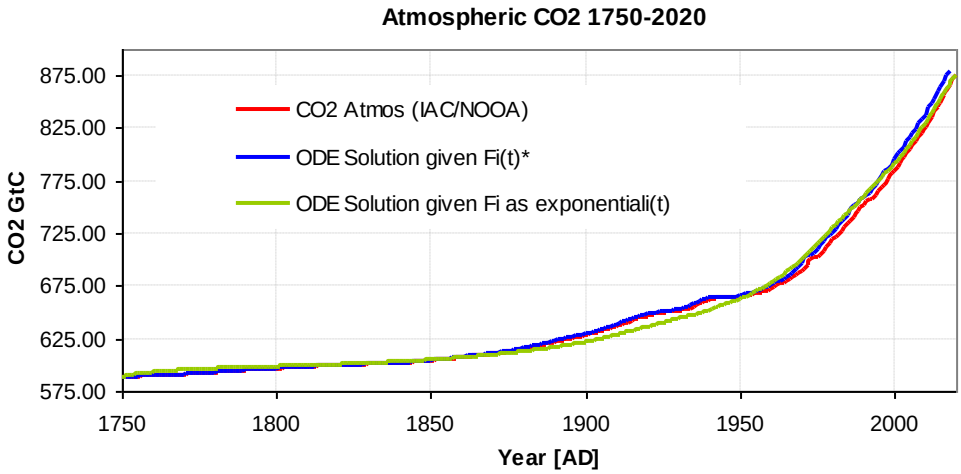

Figure 10. Atmospheric CO_2 as calculated using equation (13) with Fi as derived by model (blue) and as derived from exponential fit (green), both using a time constant of 14,2 years. The rising value of Fi results in an excellent fit using a time constant of just 14.2 years (as indeed should be the case because this is the inverse problem of the model itself). The atmospheric CO_2 has been shifted by 2 years for clarity, otherwise it is barely visible.

In addition to resolving any inconsistency in the value of the time constant, the rising nature of F_i also resolves the confusion regarding a single CO_2 lifetime. For example, IPCC tabulates CO_2 lifetime as "5 to 200 yr" with note "c" stating "No single lifetime can be defined for CO_2 because of the different rates of uptake by different removal processes" (IPCC Ed., 2001, Table 1 p38). Thus, even though there may be different removal processes, it is entirely possible to determine the system behaviour using a single effective residence time for CO_2.

6. Conclusion

 doi:10.20944/preprints202205.0172.v2

This study describes a new approach to modelling the carbon cycle, which is implemented in a two-box CO_2 absolute flow model.

- The model accurately describes the values of ⊚^{14}C and $\delta^{13}C$ over 200 years, yet without assuming that bomb radiocarbon and anthropogenic carbon behave differently.
- The study shows that the claimed "Revelle Bypass" does not occur in practice because bulk exchange flows dominate isotopic ratio flows. In practice, there is therefore no significant difference in the behaviour of different isotopes, apart from fractionation.
- The study applies the airborne fraction to the calculation of residence time, with modifications to consider and include the presence of a temporal variation in bulk CO_2 exchange inflow. This modification yields the same residence time for bulk CO_2 exchange inflow as for the ^{14}C bomb pulse, showing the "Revelle Bypass" has been the cause of this confusion.
- Furthermore, the study shows that it is possible for there to be a rising influx of CO_2 from the ocean/land reservoir, and at the same time, a net sink of atmospheric CO_2.

The study overturns a key assumption of the carbon cycle, namely that "bomb radiocarbon and anthropogenic CO_2 do not behave identically." (Joos 1994). This has profound implications for our understanding of the exchange flux and climate change.

The model is available on https://geomatix.net/downloads/iso-uptake.htm

Acknowledgments: I would like to thank my colleague Dr. Andrew Layfield (Engineering and Environmental Studies), City University, Hong Kong, for his detailed comments and proofreading. The author would like to thank and acknowledge all the data providers indicated in "Data References", without whom this work could never have been carried out. This research was self-funded and received no external funding whatsoever. The author declares no conflict of interest.

Symbol Table and Acronyms

$\mathbf{t_a}$	Residence time (years)
RCO2	Relative Reservoir Size
β	Rel. proportion of CO2ff not mixing in atmosphere
Yb	Bomb Yield in megatons
$\mathbf{\Delta^{14}C_{init}}$	Initial value of $\Delta^{14}C$ at start of iteration
$\mathbf{\delta^{13}C_{init}}$, $\mathbf{\delta^{13}C_{ff}}$	The value of $\delta^{13}C$: initial isotopic ratio, fossil fuels
a	$1/\mathbf{t_a}$ yr^{-1}
A, A_{abs}, A_s	Relative, absolute standard, and specific ^{14}C activity
$A_{14}[]$, $R_{14}[]$	$^{14}C/C$ ratio: atmosphere, reservoir
AF	Airborne Fraction
$A_{FF}[]$,	Atmospheric fossil fuel content
$A_{FL}[]$, $A_{NL}[]$	Atmospheric fossil level, Natural (non-fossil) level (0-1)
B	Listed annual bomb yield (Mega Tonnes)
C	Atmospheric carbon mass, GtC
C_0	Equilibrium value of C, GtC
CO2ff	Anthropogenic fossil fuel CO_2 emissions, GtC
$F^{14}C$	^{14}C Carbon Flux, GtC yr^{-1}
F_a , F_e, F_i	Atmospheric CO_2 flux: Anthropogenic, exiting, going in GtC yr^{-1}
GCM	General Circulation Models

 doi:10.20944/preprints202205.0172.v2

GtC	Gigatonnes Carbon: equals 10^9 tonnes of carbon
M_T, M_i	Mass of mixture, Mass of portion i
R, R^{14}	Isotopic ratio, $^{14}C/C$ ratio
R_T, R_i	Ratio of a specific molecule in mixture, T and portion i
s	The exponential rate of rise of fossil fuel emissions
t_a	Time constant associated with atmospheric absorption, y_r
t_s	Time constant associated with CO2ff rise, y_r
$\Delta^{14}C$	An offset age & fractionation corrected ratio of $^{14}C/C$ †
ΔC	Change in C at each iteration, GtC
ΔT	Change in time at each iteration, y_r
δ	Isotopic ratio relative to a standard
$\delta^{13}C$	An offset measure of $^{13}C/C$ ratio relative to a standard
$\delta^{13}C_F$, $\delta^{13}C_N$	$\delta^{13}C$: For Fossil CO_2, Natural (non-fossil CO_2)
$\delta^{13}C_M$, $\delta^{13}C_W$	$\delta^{13}C$ for a Measurement, for Wood
$\delta^{14}C$	An offset measure of $^{14}C/C$ ratio relative to a standard
$\sigma_{\circledcirc\circledcirc\circledcirc}\sigma_1$, σ_2	Standard deviation of fit of time series: Total, 1, 2
(t)	Denotes a function value at time, t
[i]	Denotes the value at each iteration, i

Bold-shaded indicates the seven internal optimized parameters.

† $^{14}C/^{12}C$ ratio rel. to hypoth. value of atmosphere ^{14}C in 1950 (Stuiver & Polach, 1977).

References

Arnold, J.R., 1957. The Distribution of Carbon-14 in Nature. Tellus 9, 28–32. https://doi.org/10.1111/j.2153-3490.1957.tb01850.x

Bischof, W., 1960. Periodical Variations of the Atmospheric CO 2 -content in Scandinavia. Tellus 12, 216–226. https://doi.org/10.1111/j.2153-3490.1960.tb01303.x

Broecker, W.S., 1975. Climatic Change: Are We on the Brink of a Pronounced Global Warming? Science 189, 460–463. https://doi.org/10.1126/science.189.4201.460

Cawley, G.C., 2011. On the Atmospheric Residence Time of Anthropogenically Sourced Carbon Dioxide. Energy Fuels 25, 5503–5513. https://doi.org/10.1021/ef200914u

Dai, M., Lu, Z., Zhai, W., Chen, B., Cao, Z., Zhou, K., Cai, W.-J., Chenc, C.-T.A., 2009. Diurnal variations of surface seawater pCO2 in contrasting coastal environments. Limnol. Oceanogr. 54, 735–745. https://doi.org/10.4319/lo.2009.54.3.0735

Faassen, K.A.P., Nguyen, L.N.T., Broekema, E.R., Kers, B.A.M., Mammarella, I., Vesala, T., Pickers, P.A., Manning, A.C., Vilà-Guerau De Arellano, J., Meijer, H.A.J., Peters, W., Luijkx, I.T., 2022. Diurnal variability of atmospheric O 2 , CO 2 and their exchange ratio above a boreal forest in southern Finland (preprint). Gases/Field Measurements/Troposphere/Physics (physical properties and processes). https://doi.org/10.5194/acp-2022-504

Friedlingstein, P. et al., 2022: Global Carbon Budget 2022, Earth Syst. Sci. Data, 14, 4811–4900, https://doi.org/10.5194/essd-14-4811-2022

Gilbert Strang, Massachusetts Institute of Technology, MIT Open Courseware, Differential Equations, Response to Exponential Input, http://ocw.mit.edu/RES-18-009F15

Graven, H., Keeling, R.F., Rogelj, J., 2020. Changes to Carbon Isotopes in Atmospheric CO 2 Over the Industrial Era and Into the Future. Global Biogeochemical Cycles 34, e2019GB006170. https://doi.org/10.1029/2019GB006170

Harvey, L.D.D., 2000. Global warming: the hard science, 1. publ. ed, Pearson education. Prentice Hall, Harlow Munich. Routledge, (2018) ISBN 0582-38167-3

Heimann Martin, 1993. The Global Carbon Cycle In The Climate System. in Modelling Oceanic Climate Interactions, NATO ASI Series VolIII, Springer-Verlag, Heidelberg, 1993

Hesshaimer, V., Heimann, M., Levin, I., 1994. Radiocarbon evidence for a smaller oceanic carbon dioxide sink than previously believed. Nature 370, 201–203. https://doi.org/10.1038/370201a0

Houghton, J.T., Intergovernmental Panel on Climate Change (Eds.), 1996. Climate change 1995: the science of climate change. Cambridge University Press, Cambridge ; New York.

Hua, Q., Turnbull, J.C., Santos, G.M., Rakowski, A.Z., Ancapichún, S., De Pol-Holz, R., Hammer, S., Lehman, S.J., Levin, I., Miller, J.B., Palmer, J.G., Turney, C.S.M., 2022. ATMOSPHERIC RADIOCARBON FOR THE PERIOD 1950–2019. Radiocarbon 64, 723–745. https://doi.org/10.1017/RDC.2021.95

Intergovernmental Panel On Climate Change (Ed.) Climate Change 2001: "The Scientific Basis". Third Assesment Report, IPCC, Cambridge University Press.

Intergovernmental Panel On Climate Change (Ed.), 2013. Carbon and Other Biogeochemical Cycles, in: Climate Change 2013 – The Physical Science Basis. Cambridge University Press, pp. 465–570. https://doi.org/10.1017/CBO9781107415324.015

Intergovernmental Panel On Climate Change, 2021. Global Carbon and other biogeochemical Cycles and Feedbacks in Climate Change 2021 – The Physical Science Basis: Working Group I Contribution to the Sixth Assessment Report of the Intergovernmental Panel on Climate Change, 1st ed. Cambridge University Press. https://doi.org/10.1017/9781009157896

Joos, F., 1994. Imbalance in the budget. Nature 370, 181–182. https://doi.org/10.1038/370181a0

Kuderer, Matthias, Samuel Hammer, and Ingeborg Levin, 2018 "The Influence of 14CO2 Releases from Regional Nuclear Facilities at the Heidelberg 14CO2 Sampling Site (1986–2014)." Atmospheric Chemistry and Physics 18, no. 11 (June 6, 2018): 7951–59. https://doi.org/10.5194/acp-18-7951-2018.

Kutschera, W., 2013. Applications of accelerator mass spectrometry. International Journal of Mass Spectrometry 349–350, 203–218. https://doi.org/10.1016/j.ijms.2013.05.023

Leinweber, A., Gruber, N., Frenzel, H., Friederich, G. E., and Chavez, F. P., 2009, Diurnal carbon cycling in the surface ocean and lower atmosphere of Santa Monica Bay, California, Geophys. Res. Lett., 36,L08601, doi:10.1029/2008GL037018.

Levin, I., Naegler, T., Kromer, B., Diehl, M., Francey, R.J., Gomez-Pelaez, A.J., Steele, L.P., Wagenbach, D., Weller, R., Worthy, D.E., 2010. Observations and modelling of the global distribution and long-term trend of atmospheric 14CO2. Tellus B: Chemical and Physical Meteorology 62, 26. https://doi.org/10.1111/j.1600-0889.2009.00446.x

Lichtfouse, E., Lichtfouse, M., Kashgarian, M., Bol, R., 2005. 14C of grasses as an indicator of fossil fuel CO2 pollution. Environ Chem Lett 3, 78–81. https://doi.org/10.1007/s10311-005-0100-4

Melillo, J.M., Butler, S., Johnson, J., Mohan, J., Steudler, P., Lux, H., Burrows, E., Bowles, F., Smith, R., Scott, L., Vario, C., Hill, T., Burton, A., Zhou, Y.-M., Tang, J., 2011. Soil warming, carbon–nitrogen interactions, and forest carbon budgets. Proc. Natl. Acad. Sci. U.S.A. 108, 9508–9512. https://doi.org/10.1073/pnas.1018189108

Naegler, T., Levin, I., 2006. Closing the global radiocarbon budget 1945–2005. J. Geophys. Res. 111, D12311. https://doi.org/10.1029/2005JD006758

Ota, M., Katata, G., Nagai, H., Terada, H., 2016. Impacts of C-uptake by plants on the spatial distribution of 14 C accumulated in vegetation around a nuclear facility—Application of a sophisticated land surface 14 C model to the Rokkasho reprocessing plant, Japan. Journal of Environmental Radioactivity 162–163, 189–204. https://doi.org/10.1016/j.jenvrad.2016.05.032

Oeschger, H., Siegenthaler, U., Schotterer, U., Gugelmann, A., 1975. A box diffusion model to study the carbon dioxide exchange in nature. Tellus A: Dynamic Meteorology and Oceanography 27, 168. https://doi.org/10.3402/tellusa.v27i2.9900

Olsen, A., Omar, A. M., Stuart-Menteth, A. C., and Triñanes, J. A., 2004, Diurnal variations of surface ocean *p*CO2 and sea-air CO2 flux evaluated using remotely sensed data, *Geophys. Res. Lett.*, 31, L20304, doi:10.1029/2004GL020583.

Palonen, V., Pumpanen, J., Kulmala, L., Levin, I., Heinonsalo, J., Vesala, T., 2018. Seasonal and Diurnal Variations in Atmospheric and Soil Air 14 CO 2 in a Boreal Scots Pine Forest. Radiocarbon 60, 283–297. https://doi.org/10.1017/RDC.2017.95

Popper, Karl. 1934. Logik der Forschung [The Logic of Scientific Discovery] (2nd ed.). Reprint 1962. La lógica de la investigación científica. Tecnos, Madrid. Reprint 1992. London: Routledge. pp. 121–132. (1992) ISBN 978-84-309-0711-3.

Revelle, R., Suess, H.E., 1957. Carbon Dioxide Exchange Between Atmosphere and Ocean and the Question of an Increase of Atmospheric CO2 during the Past Decades. Tellus 9, 18–27. https://doi.org/10.3402/tellusa.v9i1.9075

Rice, Ken; Schade, Gunnar W.; Maslin, Mark A. Comment on "World Atmospheric CO2, Its 14C Specific Activity, Non-fossil Component, Anthropogenic Fossil Component, and Emissions (1750–2018)" (Skrable et al. 2022) Health Physics 123(1):p 28-30, July 2022. | DOI: 10.1097/HP.0000000000001582

Rubino, M., Etheridge, D.M., Trudinger, C.M., Allison, C.E., Battle, M.O., Langenfelds, R.L., Steele, L.P., Curran, M., Bender, M., White, J.W.C., Jenk, T.M., Blunier, T., Francey, R.J., 2013. A revised 1000 year atmospheric δ 13 C-CO 2 record from Law Dome and South Pole, Antarctica: 1000 YEARS OF ATMOSPHERIC δ 13 C-CO 2. J. Geophys. Res. Atmos. 118, 8482–8499. https://doi.org/10.1002/jgrd.50668

Sarmiento, Jorge L., Gruber Nicolas., 2002. Sinks for Anthropogenic Carbon. Physics Today August 2002.

Siegenthaler, U., Oeschger, H., 1987. Biospheric CO2 emissions during the past 200 years reconstructed by deconvolution of ice core data. Tellus B: Chemical and Physical Meteorology 39, 140. https://doi.org/10.3402/tellusb.v39i1-2.15331

Stenström, K, Skog, G, Georgiadou, E, Genberg, J & Mellström, A. 2011. A guide to radiocarbon units and calculations. LUNFD6(NFFR-3111)/1-17/(2011), Lund University,

Stuiver, M., Polach, H.A., 1977. Discussion Reporting of 14 C Data. Radiocarbon 19, 355–363. https://doi.org/10.1017/S0033822200003672

Stuiver, M., Quay, P.D., 1981. Atmospheric 14C changes resulting from fossil fuel CO2 release and cosmic ray flux variability. Earth and Planetary Science Letters 53, 349–362. https://doi.org/10.1016/0012-821X(81)90040-6

Stuiver, M., Reimer, P.J., Bard, E., Beck, J.W., Burr, G.S., Hughen, K.A., Kromer, B., McCormac, G., Van Der Plicht, J., Spurk, M., 1998. INTCAL98 Radiocarbon Age Calibration, 24,000–0 cal BP. Radiocarbon 40, 1041–1083. https://doi.org/10.1017/S0033822200019123

Suess, H.E., 1955. Radiocarbon Concentration in Modern Wood. Science 122, 415–417. https://doi.org/10.1126/science.122.3166.415.b

Svetlik, I., Povinec, P.P., Molnár, M., Meinhardt, F., Michálek, V., Simon, J., Svingor, É., 2010. Estimation of Long-Term Trends in the Tropospheric 14 CO 2 Activity Concentration. Radiocarbon 52, 815–822. https://doi.org/10.1017/S0033822200045835

Takahashi, H.A., Konohira, E., Hiyama, T., Minami, M., Nakamura, T., Yoshida, N., 2002. Diurnal variation of CO2 concentration, Δ14C and δ13C in an urban forest: estimate of the anthropogenic and biogenic CO2 contributions. Tellus B: Chemical and Physical Meteorology 54, 97. https://doi.org/10.3402/tellusb.v54i2.16651

Tans, P.P., Berry, J.A., Keeling, R.F., 1993. Oceanic 13 C/ 12 C observations: A new window on ocean CO 2 uptake. Global Biogeochemical Cycles 7, 353–368. https://doi.org/10.1029/93GB00053

Tans, P., 2022. Reminiscing On The Use And Abuse Of 14C And 13C In Atmospheric CO2. Radiocarbon 64, 747–760. https://doi.org/10.1017/RDC.2022.7

Data References

D1. Institute for Atmospheric and Climate Science (IAC), CO2 Mean Global AD0 to AD2014 ftp://data.iac.ethz.ch/CMIP6/input4MIPs/UoM/GHGConc/CMIP/yr/atmos/UoM-CMIP-1-1-0/GHGConc/gr3-GMNHSH/v20160701/ mole_fraction_of_ carbon_dioxide_in_air_input4MIPs_GHGConcentrations_CMIP_UoM-CMIP-1-1-0_gr3-GMNHSH_0000-2014.csv

D2. NOOAA GML. Accessed 04-March-2022. https://gml.noaa.gov/ccgg/trends/gl_data.html File: https://gml.noaa.gov/webdata/ccgg/trends/co2/co2_annmean_gl.txt

D3. Global Carbon Budget: National_Carbon_Emissions_2021v0.4.xlsx Historical Budget, Global Fossil Emissions Visited 04 March 2022. Friedlingstein et al (2021),

D4. World Data Service for Paleoclimatology, Boulder and NOAA Paleoclimatology Program, National Centers for Environmental Information (NCEI) https://www1.ncdc.noaa.gov/pub/data/paleo/icecore/antarctica/law/law2018d13c-co2.txt, https://doi.org/10.25919/5bfe29ff807fb

D5. UNSCEAR: United Nations Scientific Committee on the Effects of Atomic Radiation 2000 Report To The General Assembly. Volume I: Sources. Annex C: Exposures To The Public From Man-Made Sources Of Radiation 207 Sources And Effects Of Ionizing Radiation. Table 4. Annual Fission And Fusion Yields.

D6. Calib: INTCAL20/SGCAL20. Stuiver, M. et al, 2022 CALIB 8.2 [WWW program] at http://calib.org, accessed 2022-3-4 Rev 8.1.0 intcal20.14c, shcal20.14c

D7. HADCRUT4, https://www.metoffice.gov.uk/hadobs/

D8. hadcrut4 /data/current/time_series/ HadCRUT.4.6.0.0.monthly_ns_avg.txt, hadsst4/data/csv/ HadSST.4.0.0.0_monthly_GLOBE.csv

 doi:10.20944/preprints202205.0172.v2

disclaim responsibility for any injury to people or property resulting from any ideas, methods, instructions or products referred to in the content.